RAPID COMMUNICATIONS IN MASS SPECTROMETRY
Rapid Commun. Mass Spectrom. 2006; **20**: 1838–1844
Published online in Wiley InterScience (www.interscience.wiley.com) DOI: 10.1002/rcm.2520

RCM

Combined infrared multiphoton dissociation and electron-capture dissociation using co-linear and overlapping beams in Fourier transform ion cyclotron resonance mass spectrometry

Romulus Mihalca[1], Yuri E. M. van der Burgt[1], Liam A. McDonnell[1], Marc Duursma[1], Iliya Cerjak[1], Albert J. R. Heck[2] and Ron M. A. Heeren[1,2*]

[1]FOM Institute for Atomic and Molecular Physics (AMOLF), Kruislaan 407, 1098 SJ Amsterdam, The Netherlands
[2]Department of Biomolecular Mass Spectrometry, Bijvoet Center for Biomolecular Research, Utrecht Institute for Pharmaceutical Sciences, Utrecht University, Sorbonnelaan 16, 3584 CA Utrecht, The Netherlands

Received 15 February 2006; Revised 30 March 2006; Accepted 31 March 2006

A novel set-up for Fourier transform ion cyclotron resonance mass spectrometry (FTICR) is reported for simultaneous infrared multiphoton dissociation (IRMPD) and electron-capture dissociation (ECD). An unmodified electron gun ensures complete, on-axis overlap between the electron and the photon beams. The instrumentation, design and implementation of this novel approach are described. In this configuration the IR beam is directed into the ICR cell using a pneumatically actuated mirror inserted into the ion-optical path. Concept validation was made using different combinations of IRMPD and ECD irradiation events on two standard peptides. The ability to perform efficient IRMPD, ECD and especially simultaneous IRMPD and ECD using lower irradiation times is demonstrated. The increase in primary sequence coverage, with the combined IRMPD and ECD set-up, also increases the confidence in peptide and protein assignments.

Proteomics is an indispensable technology in the molecular description of life's organization. As proteins carry out most biological activities in a cell or organism,[1] it is essential to characterize their structure, expression, distribution and interactions. Over the past decade mass spectrometry (MS) has become the method of choice for the systematic analysis of a proteome. It has enabled protein identification and quantification, protein profiling, and the characterization of protein interactions and modifications. Nevertheless, MS-based proteomics still faces significant challenges,[1,2] such as the improvement of tandem mass (MS/MS) spectra in order to decrease the amount of false positives in peptide and protein assignments. Here we describe an instrumental development to improve the quality and information content of MS/MS spectra.

A common method of protein identification uses partial sequence information of one or more proteolytic peptides.[1,3,4] This sequence-tag strategy involves proteolysis of the protein mixture, followed by chromatographic separation of peptides and MS/MS. The peak lists from such MS/MS spectra are then submitted to a database for protein identification.

The confidence of the assignment increases with the amount of sequence information and the mass accuracy of the measurement. The high mass accuracy provided by Fourier transform ion cyclotron resonance mass spectrometry (FTICRMS) is the principal reason for it currently being the method of choice for proteomics investigations.[4] With suitable control, FTICRMS can provide mass accuracies consistently under 2 ppm, and the majority under 1 ppm.[5–7] While the new Orbitrap can also provide accurate mass capabilities,[8] the process of FTICRMS permits the analyst to use a wide variety of tandem mass spectrometry techniques. Collision-activated dissociation (CAD),[9,10] infrared-multiphoton dissociation (IRMPD),[11,12] ultraviolet photodissociation (UVPD),[13,14] and electron-capture dissociation (ECD)[15–19] can all be used to obtain sequence information. The identity and relative signal intensities of the product ions are dependent on which technique is used and how it is applied. This flexibility has been exploited to the extent that entire proteins have been sequenced using a combination of these MS/MS techniques, even including the position of post-translational modifications (PTMs).[20]

For typical sequence-tag proteomics experiments, involving a separation step, MS/MS must be performed on a

Correspondence to: R. M. A. Heeren, FOM Institute for Atomic and Molecular Physics, Kruislaan 407, 1098 SJ Amsterdam, The Netherlands.
E-mail: heeren@amolf.nl
Contract/grant sponsor: Nederlandse organisatie voor Wetenschappelijk Onderzoek (NWO).

time-scale compatible with the separation. A scan duration of less than 2 s would allow the MS/MS spectra to be obtained from several co-eluting peptides (assuming liquid chromatography (LC) peak duration of 10–30 s). IRMPD and ECD are both well established, easy to implement and have time-scales compatible with LC/MS proteomics.

1. IRMPD—Irradiation heating times are usually 10^2 to 10^3 ms. Peptide and protein ions undergo fragmentation typical of slow vibrational activation.[21] Labile PTMs are generally lost prior to backbone cleavage and efficient backbone cleavage forms abundant *b* and *y* ions. The mass losses due to the loss of a labile group, such as a glycan or phosphate, can be used to indicate the presence of that group.[18] Occasionally, the position of the modification can be determined from established biochemical rules. In comparison with ECD, IRMPD allows fragmentation of singly charged ions and provides N-terminal cleavages of the proline residue.
2. ECD—Involves the capture of low-energy electrons by multiply charged molecule-related ions of peptides and proteins, e.g. $[M+nH]^{n+}$. ECD can provide extensive sequence information and is the only technique to retain labile side groups such as PTMs.[22] Consequently, it is the only MS technique able to identify *and* locate PTMs. This ability led to early reports speculating that ECD might be a non-ergodic process.[15] The gentle nature of ECD has been further demonstrated by the observation that non-covalent interactions can limit the degree of fragmentation *observed* with ECD. More abundant product ions and more extensive sequence information are obtained by gently heating the ions during ECD using collisional[23] or IR[24] activation.

It is desirable to have simultaneous access to ECD and IRMPD. However, both techniques are optimized when the electron/IR beam has complete overlap with the ion cloud in the ICR cell. Figure 1(a) shows a schematic of a typical FTICR instrument, including the distribution of an ion cloud. As can be seen, the ions are transferred from an external ion source by ion-optical elements to the ICR cell, which is situated in the center of a strong magnetic field. Here, ions form an ellipsoid along the axis of the ICR cell. Co-axial irradiation of this ion packet by the electron beam *and* the IR beam is complicated by the ion optics on the front side of the ICR cell; consequently, previous attempts have concentrated on introducing both beams from the rear. Figures 1(b)–1(e) show the solutions to date, but all of these compromise the degree of overlap with the ion cloud for one of the beams.

The first attempts to apply the complementary capabilities of ECD and IRMPD were made by Håkansson *et al.*[18] A directly heated filament placed off-axis combined with an on-axis IR laser beam (Fig. 1(b)) was used to characterize several post-translationally modified peptides. This configuration allowed efficient IRMPD but satisfactory ECD spectra required long irradiation times, up to 30 s, because of poor overlap between the ion cloud and the small electron beam produced by the filament cathode. The broader electron beam produced by an indirectly heated dispenser cathode provides more overlap and thus increased ECD efficiency; however, performance is still sensitive to position,

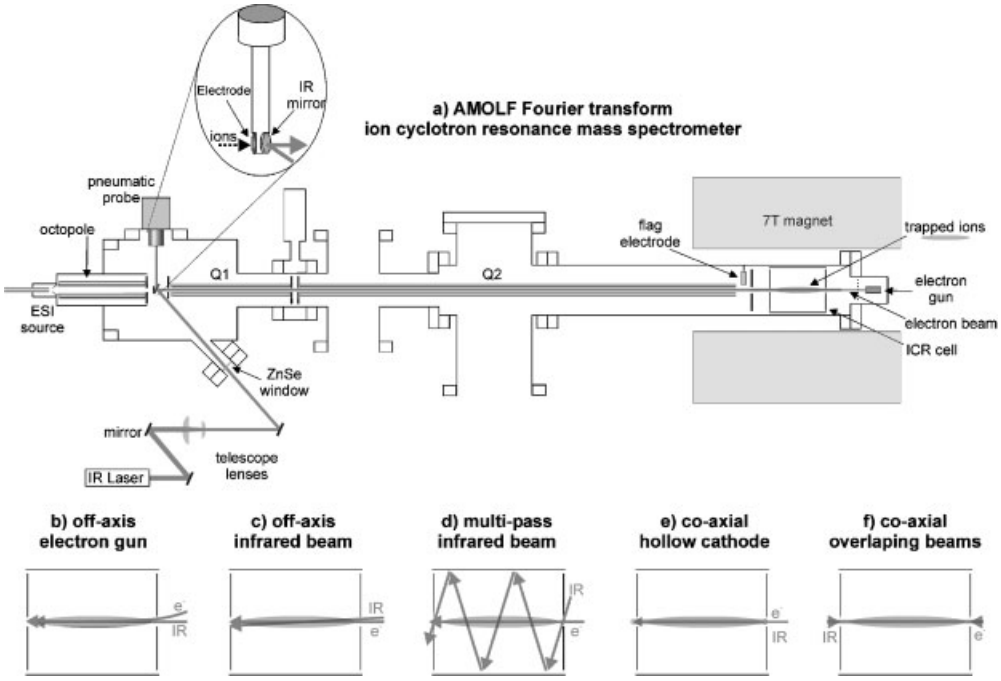

Figure 1. (a) Schematic of the FTICR mass spectrometer at AMOLF including the probe, and displaying the paths of the IR laser and electron beam. Not to scale. (b–e) Existing solutions for simultaneously irradiating an ion cloud trapped in the ICR cell with an IR beam and an electron beam. Only the co-axial overlapping beams provided with this pneumatic probe design (f) ensure overlap between the ion cloud, IR beam and electron beam.

DOI: 10.1002/rcm

decreasing rapidly when the electron gun is moved more then a few millimeters off-axis.

Alternative designs have positioned the electron gun on-axis and the IR beam slightly off-axis (Figs. 1(c) and 1(d)).[24] Using this configuration more abundant product ions have been reported. Nevertheless, overlap of the IR beam with the ion cloud is incomplete. Recently Tsybin *et al*. implemented a ring cathode in which the IR laser passes through the center hole (Fig. 1(e)).[25] Short irradiation times for combined IRMPD and ECD provided more than 60% sequence coverage of the peptide HNP-1. In the strong magnetic field the electron beam maintains the ring cross section of the cathode throughout the ICR cell. Therefore, with this configuration, the ion cloud and electron beam have just a boundary interaction region. ECD efficiency could be increased by increasing the effective interaction volume. This can be achieved by using sidekick trapping or ion-excitation with an off-resonance excitation. However, such excitation would reduce IR overlap.

All the instrumental configurations mentioned above compromise the degree of overlap between the ion cloud and either the IR or electron beam. The common cause is the combined introduction of the IR and electron beam from the rear end of the ICR cell.

Here we report a novel FTICRMS set-up for combined on-axis ECD and IRMPD in the ICR cell, in which both beams have complete overlap with the ion cloud (Figs. 1(a) and 1(f)), using a standard dispenser cathode. An IR mirror, attached to a guided pneumatic probe, is inserted between ion-optical elements to reflect the IR beam along the axis of the instrument and into the ICR cell. Geometrical design ensures good overlap between the electron beam, IR beam and ion cloud. A detailed description of this new device is presented followed by validation of the approach.

DESIGN AND EXPERIMENTAL

Experimental set-up

All the experiments were performed using a heavily modified Bruker APEX 7.0eT FTICR mass spectrometer equipped with an infinity cell, a 7 T super-conducting magnet and an electron source located behind the ICR cell. Figure 1(a) shows a schematic of the instrument. The ions generated by an electrospray ionization (ESI) source are accumulated in an octopole ion trap prior to being transferred to the ICR cell via two quadrupole ion guides. As can be seen, there is a clear optical path through the quadrupole ion guides and into the ICR cell. It is evident from this figure that, once an IR beam is aligned through the cell and quadrupole ion guides, and the electron source has been positioned for maximum current (using the movable 'flag electrode' on the opposite side of the cell), the geometry dictates that the beams are co-axial and will overlap with the ions contained in the center of the ICR cell.

The key to this approach is the ability to direct the IR beam through the quadrupole ion guides after the ions have been transferred to the ICR cell, specifically, the ability to align the IR laser beam along the axis, and the reproducibility of this optimum alignment. With these concerns in mind, a pneumatic probe has been designed that inserts an IR first-surface mirror in front of the quadrupole ion guides, includes a mechanical auto-alignment mechanism and allows the user to fine-tune the position and angle of the IR mirror.

Pneumatic probe

After ion transfer to the ICR cell an IR mirror, attached to the pneumatic probe, is inserted between ion-optical elements to direct the IR beam into the center of the ICR cell. The schematic of the instrument (Fig. 1(a)) indicates the paths of the IR beam and electron beam. Behind the IR mirror, an electrically isolated metallic plate is also attached to the probe. While the probe is inserted, it is used to monitor the current emitted from the octopole.

Figure 2 details the principal elements of the probe. The probe is a stainless steel rod, to which the IR first-surface mirror and the electrically isolated electrode are attached. The mirror has been designed to redirect an incident laser beam through 49.8° azimuthal onto the ion-optical axis (this angle was defined by the available vacuum flanges). A first-

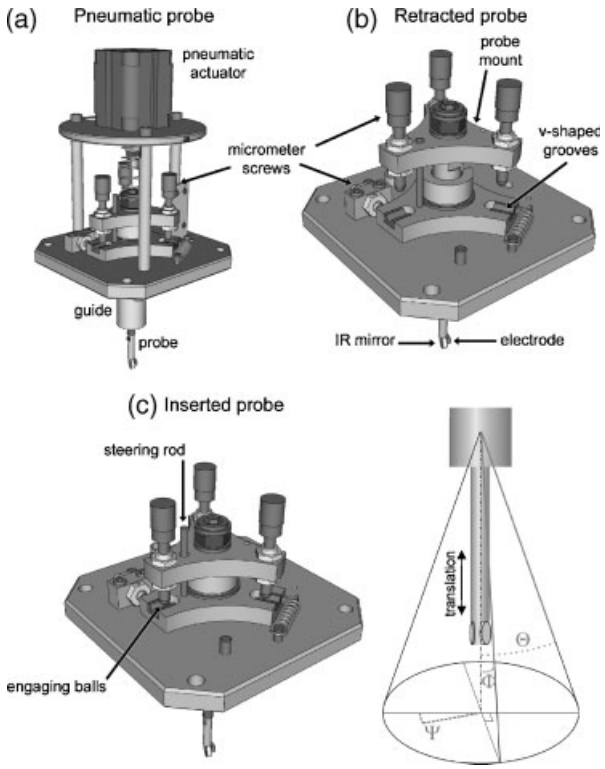

Figure 2. Schematics of the pneumatic probe, highlighting the principal components, its mode of action and the degrees of freedom. Retraction of the probe lifts the mount and three micrometer screws (b). The bottoms of these micrometer screws consist of 'engaging balls'. On insertion (c), the engaging balls enter three corresponding v-shaped grooves. This fixes the position of the probe. Variation of the three screws provides up to 10 mm axial translation and 2.5° freedom in the pitch and roll angles of the probe, Θ and Φ. A fourth micrometer screw (b) can rotate the plate containing the three v-shaped grooves, and thus the yaw angle of the mirror and probe, by up to ±5° (Ψ).

DOI: 10.1002/rcm

surface mirror reflects light from its front surface. The use of a first-surface mirror avoids the secondary reflections of a standard mirror (reflection occurs from the front surface and rear coating) and the beam displacement due to refraction through the glass of the mirror.

Accurate positioning of the 'in' position of the IR mirror and the high reproducibility of this final position are based on a mechanical auto-alignment mechanism. Figure 2 also illustrates this mode of action. The probe is rigidly attached to a mounting that sits upon three lockable micrometer screws. Retraction of the probe by the pneumatic actuator lifts this entire assembly: the probe, the mounting and the three micrometer screws. The bottoms of these screws consist of small metallic spheres, or engaging balls.

When the probe is released, the three engaging balls enter three corresponding v-shaped grooves (Fig. 2(b)). A small rod ensures that the engaging balls enter the grooves and atmospheric pressure ensures that these spheres sit at the base of these grooves. Consequently, the lateral position of the probe is defined and reproducible. Variation of the three micrometer screws provides up to 10 mm axial translation freedom and up to 2.5° freedom in the two elevation angles of the probe, Θ and Φ (Fig. 2). A fourth micrometer screw can be used to rotate the plate containing the three v-shaped grooves by up to ±5° azimuthal (Ψ in Fig. 2). Accordingly, these four micrometer screws allow all three angles and the axial position of the probe to be fine-tuned. When the probe is retracted, the mirror and mount with the three micrometer screws are lifted, thereby not affecting the inserted position of the probe. A guide ensures the smooth motion of the probe through the duration of its insertion and extraction.

Prior to the probe being mounted the stability of the positioning system was tested using a HeNe alignment laser over a 4 m working distance. The position of the laser spot was found to be identical after hundreds of laser shots. Further use has confirmed the stability of the probe for extended periods of time. Similar devices have been reported to provide a mean angular error of 3 μR.[26]

IR irradiation

IRMPD and the simultaneous IRMPD and ECD experiments were performed using a 10.6 μm CO_2 laser (model J48-2; Synrad, Mukiteo, WA, USA). The continuous laser pulses were activated with a TTL trigger generated by the in-house software AWE 1.5.22. Laser powers of 2–2.5 W (measured after the ICR cell) and pulse durations of 50–1500 ms have all provided efficient IR activation. For improved transmission a telescope was used to reduce the diameter of the IR beam to approximately 1.2 mm prior to it entering the mass spectrometer through a ZnSe window (see Fig. 1(a)).

Electron irradiation

An indirectly heated cathode (HeatWave, Watsonville, CA, USA) was used for the production of 320 nA of 0.45 eV electrons. When not in use electron irradiation was prevented by positively biasing the dispenser cathode and applying a retarding potential to a grid located 5 mm in front of the cathode (for efficient electron extraction during ECD this grid was switched to +10 V).

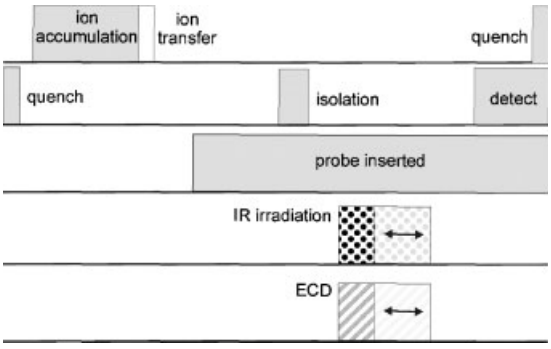

Figure 3. Schematic of the experimental sequence.

Mass spectrometry

Substance P and mellitin were purchased from Sigma Aldrich (St. Louis, MO, USA) and used without further purification. Solutions of 20 μM in 69:29:2 methanol/water/acetic acid were electrosprayed using New Objective Picotips™ at 20 μL h^{-1}. Figure 3 shows a (not-to-scale) schematic of the experimental sequence. Ions produced by the ESI source were accumulated for 30 ms in the accumulation octopole[27] and subsequently ejected into the ICR cell. Multiply charged cations were trapped in the infinity ICR cell by using Ar as a trapping gas. Sidekick trapping was avoided to ensure that the ions remained on-axis but this lengthened the experimental sequence to ≈5 s (without trapping gas, experiments can be performed in 1–2 s). The ions of substance P, $[M+2H]^{2+}$ at m/z 674.372, and mellitin, $[M+4H]^{4+}$ at m/z 712.196, were isolated using a stored waveform inverse Fourier transformed (SWIFT) excitation pulse.[28]

RESULTS AND DISCUSSION

Two well-characterized peptides, substance P and mellitin, were used to determine the performance of our set-up. After isolation of the precursor ions, $[M+2H]^{2+}$ for substance P and $[M+4H]^{4+}$ for mellitin, MS/MS experiments were carried out with varying electron- and photon-irradiation times. All other experimental parameters were kept constant to enable the comparison of independent experiments with simultaneous electron and photon irradiation.

Independent and simultaneous ECD and IRMPD of substance P

In the independent ECD experiment of substance P the optimum electron-irradiation time with respect to the number of primary sequence ions and their signal intensities was experimentally determined at 1.5 s (±0.1 s). In agreement with previous results, seven c-fragments, c_4–c_{10}, and one weak z-fragment, z_9, were observed (Fig. 4).[19,29,30] As expected, due to the presence of two prolines, c_1 and c_3 were not detected. Thus, the sequence coverage of 80% corresponds to the maximum that is achievable from typical ECD fragmentation of substance P. In the independent IRMPD experiment of substance P the optimal photon-irradiation time was determined at 0.5 s (±0.1 s). Generally, the fragment signal intensities in the IRMPD spectra were higher than in the ECD spectra. Following IRMPD, six b ions

DOI: 10.1002/rcm

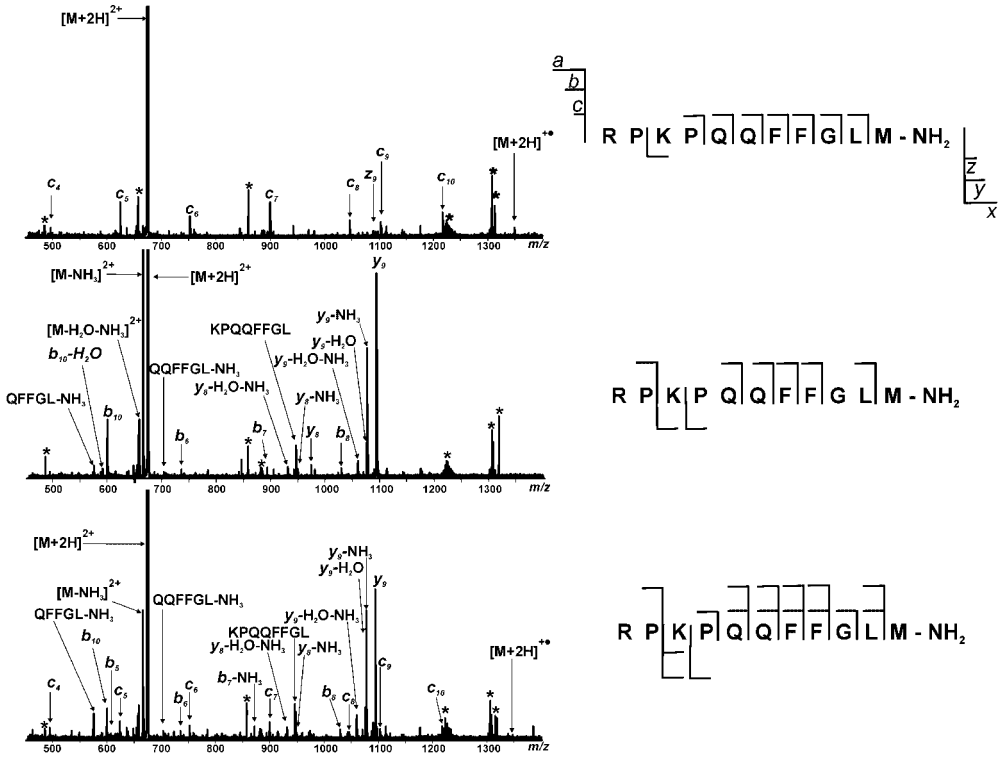

Figure 4. MS/MS spectra of the $[M+2H]^{2+}$ ion of substance P subjected to: ECD (top), IRMPD (middle) and simultaneous on-axis IRMPD and ECD (bottom). Asterisk denotes noise. Each spectrum results from the accumulation of 50 scans.

(b_2, b_5–b_8, b_{10}) and two y ions (y_8, y_9) of substance P were seen. In addition, several ions due to secondary cleavages, i.e. small neutral mass losses and internal fragments, were detected. Without including these lower abundance ions the sequence coverage from the independent IRMPD experiment was 70%. As can be seen in Fig. 4, simultaneous IRMPD and ECD of doubly protonated substance P yielded all the fragments that were produced in independent ECD and IRMPD experiments. The combination of all typical ECD fragments with the y_8 fragments results in sequence coverage of 90% of substance P. The c and z ions in the simultaneous experiment were slightly less abundant than in the independent ECD spectrum.

Independent and simultaneous ECD and IRMPD of mellitin

In the ECD experiment of quadruply protonated mellitin, lower electron-irradiation times, 0.5 s, were necessary because electron-capture efficiency increases with the square of the charge.[16] A typical ECD spectrum of mellitin is shown in Fig. 5. Here, six c ions (c_9, c_{10}, c_{12}, c_{23}–c_{25}), eight z ions (z_3, z_8, z_{12}, z_{14}, z_{16}, z_{19}, z_{20}, z_{23}) and five y ions (y_{14}, y_{15}, y_{17}, y_{19}, y_{24}) were detected after 0.5 s of electron irradiation, as well as two triply protonated reduced species ($[M+4H]^{3+\bullet}$ and $[M+4H]^{3+\bullet}$–NH_3). Most of these c, z and y ions are consistent with previous results.[31] In total, these 19 ECD ions result in 52% sequence coverage. When mellitin is subjected to IRMPD for 0.5 s, four b ions (b_9, b_{10}, b_{12}, b_{23}) and 19 y ions (y_3, y_5, y_8,y_{10}, y_{11}, y_{13}–y_{21}, y_{24}) are observed. The resulting sequence coverage from these ions is 60%. In addition, multiple ions that result from neutral losses from b and y ions are present. As was the case for substance P, the IRMPD fragments of mellitin are more abundant than the ECD fragments. In all experiments product ion abundances were calculated relative to the precursor ion. After simultaneous IRMPD and ECD of mellitin for 0.5 s, three c ions (c_{10}, c_{22}, c_{25}), four z ions (z_{24}, z_{23}, z_{16}, z_{14}), 11 b ions (b_5, b_6, b_8–b_{13}, b_{19}, b_{22}, b_{23}) and 22 y ions (y_3, y_4, y_5, y_8–y_{21}, y_{24}) are observed (Fig. 5). This results in 88% sequence coverage, which is significantly higher than in the independent experiments at similar irradiation times (52% for ECD and 60% for IRMPD). However, compared with the independent experiments, some c and z ions disappeared and new b and y ions were generated. Additionally, ions that result from neutral losses from b and y ions are more abundant than in independent IRMPD. In general, the abundances of c and z ions decrease upon simultaneous irradiation whereas the abundances of b and y ions are significantly higher. To a lesser extent this change in fragmentation pathways was also seen in the simultaneous experiment of substance P. Possibly the ion cloud in the ICR cell is focused by the electron beam, resulting in a larger fraction of the precursor ions overlapping with the IR beam and thus more abundant b and y ions. IR dissociation of c and z ions would lower their abundances, as observed in the simultaneous IRMPD and ECD experiments. An alternative explanation for the increase of the relative abundance of b and y ions in the simultaneous experiments is capture of one or two electrons by the $[M+4H]^{4+}$ precursor, followed by typical b/y fragmentation upon IR irradiation.[32] This pre-activation of the IRMPD reaction pathways is in agreement with the observed decrease in the abundance of the reduced triply charged ion $[M+4H]^{3+\bullet}$ upon constant ECD irradiation and increasing IR irradiation times.

DOI: 10.1002/rcm

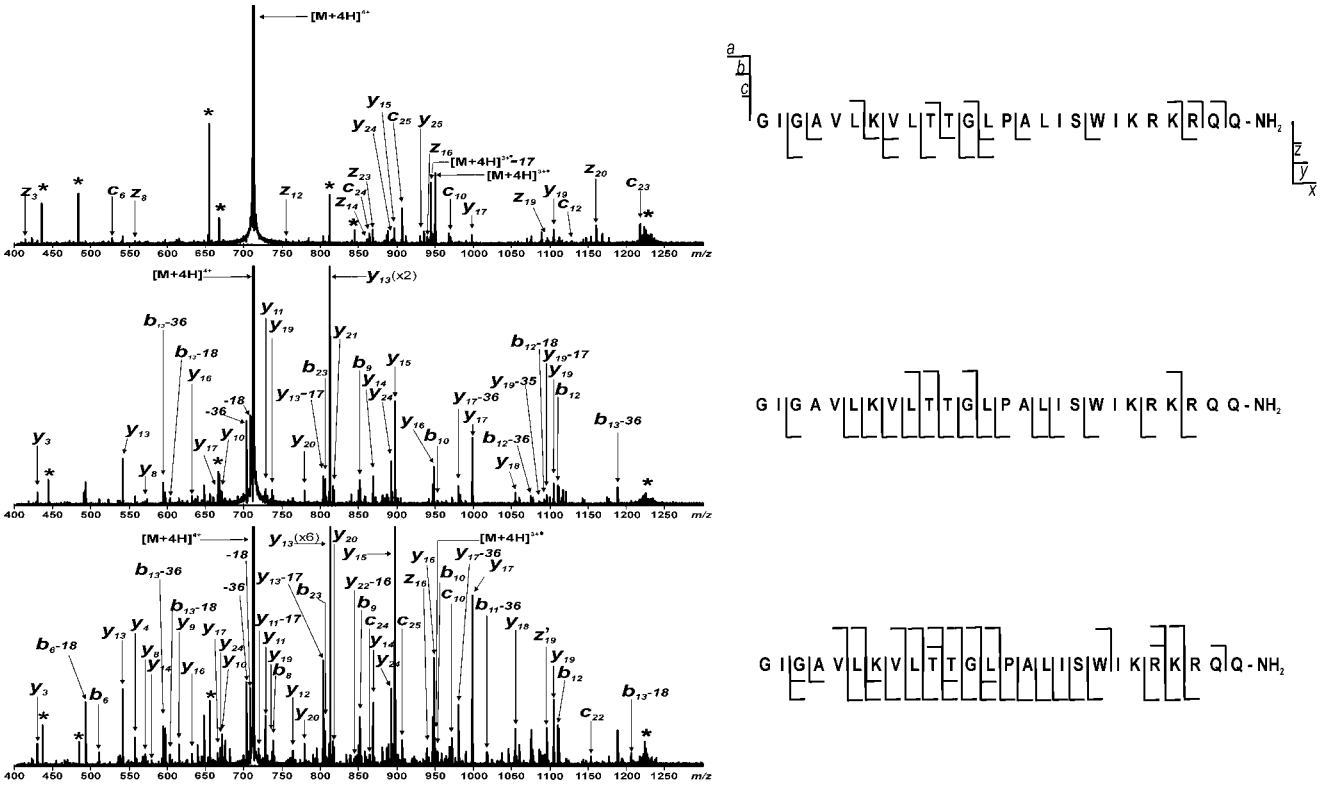

Figure 5. MS/MS spectra of the $[M+4H]^{4+}$ ion of bee venom mellitin subjected to: ECD (top), IRMPD (middle) and simultaneous on-axis IRMPD and ECD (bottom). Asterisk denotes noise. Increased sequence coverage is obtained in simultaneous on-axis IRMPD and ECD (88%) compared with independent ECD (52%) or IRMPD (60%). Each spectrum results from the accumulation of 25 individual scans.

Irradiation times versus sequence coverage

The effects of the electron- and photon-irradiation times on the number of fragments and the resulting sequence coverage of mellitin are plotted in Fig. 6. The maximum sequence coverage of mellitin using ECD was 56%, using IRMPD 76% and in the simultaneous IRMPD and ECD experiment 88%. Using simultaneous irradiation this maximum was reached after 0.5 s, which was faster than with IRMPD (0.55 s) or ECD (0.8 s). Furthermore, it is clear that simultaneous irradiation results in a higher number of fragments than in the independent experiments. Note that at 0.8 s the increase in the number of fragments in the simultaneous experiment does not result in higher sequence coverage. It is the number of *primary sequence fragments* that is important, as they provide the specific sequence information. The number of *primary sequence fragments* even begins to decrease at 0.9 s due to secondary fragmentation, thus defining an optimal irradiation time in the simultaneous experiment.

Simultaneous electron and photon irradiation of mellitin (and substance P) increases the sequence coverage in one MS/MS spectrum. In the set-up reported here it is possible to perform on-axis ECD and IRMPD of isolated ions in both independent experiments as well as in simultaneous ones using irradiation times that are compatible with the time-scales of eluting LC peptides. This flexibility increases the information content of peptide tandem mass spectra for the two standard peptides used in this study.

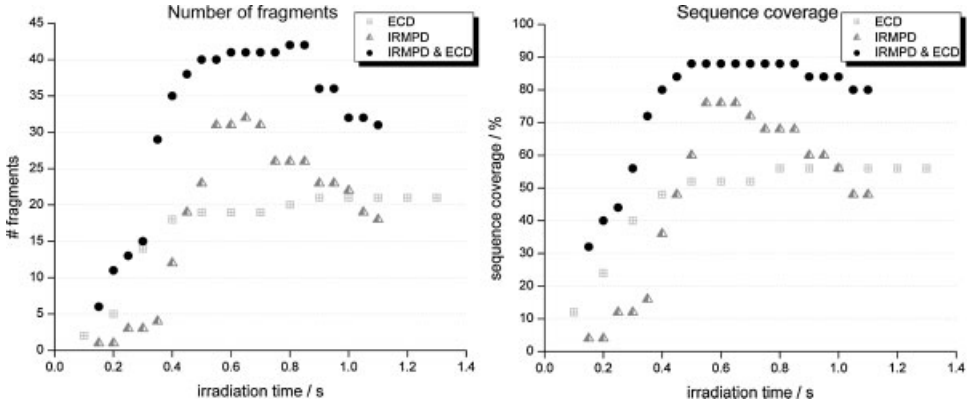

Figure 6. Plots of the number of fragments (left) and sequence coverage (right) versus irradiation time for ECD, IRMPD and simultaneous on-axis IRMPD and ECD of mellitin.

DOI: 10.1002/rcm

CONCLUSIONS

We have presented an FTICRMS set-up that allows simultaneous on-axis IRMPD and ECD in the ICR cell. In this instrumental configuration a pneumatic probe was inserted into the ion-optical path that enables on-axis IR irradiation of the ion cloud from the front of the ICR cell simultaneously with electron irradiation, provided by a standard dispenser cathode, from the rear of the ICR cell. This set-up results in a better overlap between the IR beam, electron beam and the ion cloud.

Simultaneous ECD and IRMPD resulted in a significant increase in product ions and thus sequence coverage of substance P and mellitin. The increased abundance of the *b* and *y* ions, and the dependence of this abundance on the order of IR and electron irradiation, is interpreted as ion cloud focusing by the electron beam concentrating the ion cloud on-axis and within the IR beam. This increased overlap allows shorter irradiation times. The flexibility to carry out both independent and combined ECD and IRMPD experiments, and the shorter time-scales of the combined experiments, are highly desirable for proteomics investigations because they increase the information content of the MS/MS spectra.

Acknowledgements

This work is part of research programs 49 'Mass spectrometric imaging and structural analysis of biomacromolecules' and FOM-00PR1950 'Electron capture in multiply charged proteins: dissociative recombination put to work' of the 'Stichting voor Fundamenteel Onderzoek der Materie (FOM)', which is financially supported by the 'Nederlandse organisatie voor Wetenschappelijk Onderzoek (NWO)'.

REFERENCES

1. Aebersold R, Mann M. *Nature* 2003; **42**: 198.
2. Steen H, Mann M. *Nat. Rev. Mol. Cell Biol.* 2004; **5**: 699.
3. Bergquist J, Palmblad M, Wetterhall M, Håkansson P, Markides K. *Mass Spectrom. Rev.* 2002; **21**: 2.
4. Bogdanov B, Smith RD. *Mass Spectrom. Rev.* 2004; **24**: 168.
5. Bruce JE, Anderson GA, Wen J, Harkewicz R, Smith RD. *Anal. Chem.* 1999; **71**: 2595.
6. Bruce JE, Anderson GA, Brands MD, Pasa-Tolic L, Smith RD. *J. Am. Soc. Mass Spectrom.* 2000; **11**: 416.
7. Spengler B. *J. Am. Soc. Mass Spectrom.* 2004; **15**: 703.
8. Hu Q, Noll RJ, Li H, Makarov A, Hardman M, Cooks RG. *J. Mass Spectrom.* 2005; **40**: 430.
9. Gauthier JW, Trautman TR, Jacobsen DB. *Anal. Chim. Acta* 1991; **246**: 211.
10. Senko MW, Speir JP, McLafferty FW. *Anal. Chem.* 1994; **66**: 2801.
11. Little DP, Spier JP, Senko MW, O'Connor PB, McLafferty FW. *Anal. Chem.* 1994; **66**: 2809.
12. Li W, Hendrickson CL, Emmet MR, Marshall AG. *Anal. Chem.* 1999; **71**: 4397.
13. Bowers WD, Delbert S-S, Hunter RL, McIver RT Jr. *J. Am. Chem. Soc.* 1984; **106**: 7288.
14. Williams ER, Furlong JJP, McLafferty FW. *J. Am. Soc. Mass Spectrom.* 1990; **1**: 288.
15. Zubarev RA, Kelleher NL, McLafferty FW. *J. Am. Chem. Soc.* 1998; **120**: 3265.
16. Zubarev RA, Horn DM, Fredricksson EK, Kelleher NL, Kruger NA, Lewis MA, Carpenter BK, McLafferty FW. *Anal. Chem.* 2000; **72**: 563.
17. Zubarev RA. *Mass Spectrom. Rev.* 2003; **22**: 57.
18. Håkansson K, Cooper JH, Emmet MR, Costello CE, Marshall AG, Nilsson CL. *Anal. Chem.* 2001; **73**: 4530.
19. Håkansson K, Emmett MR, Hendrickson CL, Marshall AG. *Anal. Chem.* 2001; **73**: 3605.
20. Forbes AJ, Patrie SM, Taylor GK, Kim YB, Jiang LH, Kelleher NL. *Proc. Natl. Acad. Sci. USA* 2004; **101**: 2678.
21. McLuckey SA, Goeringer DE. *J. Mass Spectrom.* 1997; **32**: 461.
22. Kelleher NL, Zubarev RA, Bush K, Furie B, Furie BC, McLafferty FW, Walsh CT. *Anal. Chem.* 1999; **71**: 4250.
23. Horn DM, Ge Y, McLafferty FW. *Anal. Chem.* 2000; **72**: 4778.
24. Håkansson K, Chalmers MJ, Quinn JP, McFarland MA, Hendickson CL, Marshall AG. *Anal. Chem.* 2003; **75**: 3256.
25. Tsybin YO, Witt M, Baykut G, Kjeldsen F, Håkansson P. *Rapid Commun. Mass Spectrom.* 2003; **17**: 1759.
26. Koster MP. *Constructieprincipies voor het nauwkeurig bewegen en positioneren*. Twente University Press: Enschede, 1998.
27. Taban IM, McDonnell LA, Rompp A, Cerjak I, Heeren RMA. *Int. J. Mass Spectrom.* 2005; **244**: 135.
28. Guan S, Marshall AG. *Int. J. Mass Spectrom. Ion Processes* 1996; **157/158**: 5.
29. Axelsson J, Palmblad M, Hakansson K, Hakansson P. *Rapid Commun. Mass Spectrom.* 1999; **13**: 474.
30. Mihalca R, Kleinnijenhuis AJ, McDonnell LA, Heck AJR, Heeren RMA. *J. Am. Soc. Mass Spectrom.* 2004; **15**: 1869.
31. Polfer NC, Haselmann KF, Zubarev RA, Langridge-Smith PRR. *Rapid Commun. Mass Spectrom.* 2002; **16**: 936.
32. Kleinnijenhuis AJ, Heck AJR, Duursma MC, Heeren RMA. *J. Am. Soc. Mass Spectrom.* 2005; **16**: 1595.

DOI: 10.1002/rcm